Effects of Electrostatic Fields and Potentials on the Electronic Energies of Conjugated Organic Molecules

Bryan E. Kohler and Jörg C. Woehl*

Department of Chemistry, University of California, Riverside, California 92521-0403

Received: October 5, 1998; In Final Form: December 15, 1998

Spectroscopic experiments that study the effect of an externally applied electric field on transition energies provide a wealth of information if carried out under high-resolution conditions. We present experimental data for octatetraene incorporated into two alkane hosts, *n*-hexane and *n*-heptane, where persistent holes burned into the lowest lying electronic singlet transition serve as precise transition frequency markers. To access the information contained in these data, we use molecular mechanics simulations to arrive at microscopic models for the guest−host geometries and calculate the internal and polarization potentials of the structures. A general model describing how molecular electronic energy levels are affected by an arbitrary distribution of electrostatic fields and potentials over the size of a probe molecule is presented and applied to a simple π-electron model that accurately reproduces the electronic energies of linear polyenes. On this basis, the hole profiles are calculated and compared to the experimental results, leading to a microscopic picture of the guest−host structures and molecular electrostatic fields.

1. Introduction

Atoms and molecules, the building blocks of matter, consist of electrically charged electrons and nuclei and interact through electrical forces. The laws of electromagnetism, together with quantum effects, govern thus all types of chemical and physical behavior, be it the making or breaking of chemical bonds, intramolecular vibrations, intermolecular attraction and repulsion and the formation of aggregates, or higher order processes such as charge transfer in biomolecules, molecular recognition (like the formation of antibody−antigen complexes during the immune reaction), or protein folding. To learn something about the origin of these forces is therefore of fundamental interest, but an experimental concept for accessing these properties with a sufficiently high spatial resolution has been missing. It is the aim of this paper to show how electrostatic fields and potentials influence the electronic energies of conjugated organic molecules serving as molecular probes of their environment and how we can, therefore, inversely extract information about *internal* electrostatic fields and potentials and their sources (namely molecular charge distributions) from spectroscopic studies.

Since the effects of externally applied electrostatic fields and potentials on the electronic transition energies of molecules are vanishingly small compared to typical absorption band line widths, it is necessary to work under high-resolution conditions. For our system, 1,3,5,7-all-*trans*-octatetraene embedded in *n*-alkane microcrystals, we chose the resolution enhancement afforded by photochemical hole burning[1] at low temperatures to obtain the required spectroscopic resolution. The photochemical holes, typically 10^4 times narrower than the whole absorption band, serve as precise frequency markers for studying the effect of an externally applied electric field on the transition energies. To gain a detailed picture of the investigated systems, we use molecular mechanics simulations to arrive at microscopic models for the guest−host geometry and analyze the experimental data with a scheme that is faithful to the actual miroscopic situation. As will be shown below, an excellent agreement between the predicted hole profiles and the experimental data can be obtained, which demonstrates the great potential of this general approach to gain a detailed view of the origin of internal electrostatic forces in a wide variety of systems.

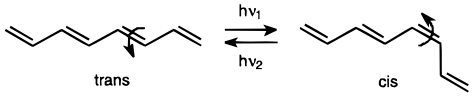

Figure 1. Photochemical cis−trans isomerization of 1,3,5,7-all-*trans*-octatetraene.

Experiments on the linear polyene octatetraene in *n*-alkane crystals are especially informative for a number of reasons. It has a well-characterized photochemical activity[2] (see Figure 1) that leads to persistent holes, namely the interconversion of trans and cis isomers[3] (which differ in their S_0-S_1 transition energy by several times their inhomogeneous bandwidths) even when embedded in an *n*-alkane crystal at liquid helium temperatures. Furthermore, the lowest lying singlet transition of a centrosymmetric all-*trans*-octatetraene is symmetry-forbidden. Even when local perturbations break the symmetry, the transition remains weak and long-lived, which results in very narrow holes. The S_1 lifetimes in *n*-alkane matrixes at liquid helium temperatures range from 100 to over 250 ns,[4,5] which means that the lifetime-limited hole widths are 3.2−1.3 MHz. These holes are suitable for determining the effects of external electric fields with great precision. But most importantly, octatetraene has a very well understood electronic structure that can be successfully described with a relatively simple model[6] based on Hückel theory, which in turn leads to especially simple expressions describing the influence of electric fields on the system. The availability of crystal structures for all-*trans*-1,3,5,7-octatetraene, *n*-hexane, and *n*-heptane leads them to lend themselves to the use of micro-

* Corresponding author. E-mail: jorg.woehl@earthling.net. Current address: Centre de Physique Moléculaire Optique et Hertzienne, CNRS et Université Bordeaux I, 351 Cours de la Libération, 33405 Talence, France.

10.1021/jp9839551 CCC: $18.00 © 1999 American Chemical Society
Published on Web 03/06/1999

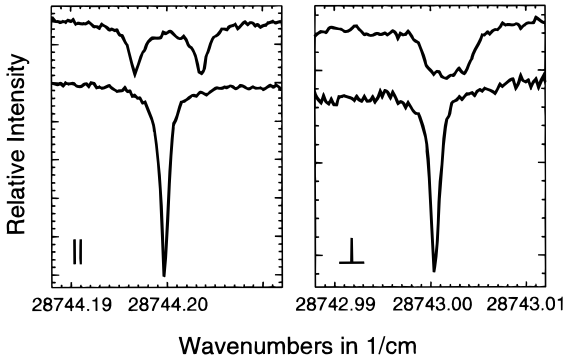

Figure 2. Polarization dependence of the hole profile of octatetraene in *n*-hexane under an applied electric field (laser light polarized parallel to the applied field in the left panel and perpendicular to the applied field in the right panel). The lower scans show the original zero-field holes; the upper scans show the hole profiles under a 2.78 kV/cm applied field. The scans appear slightly shifted because of laser drift.

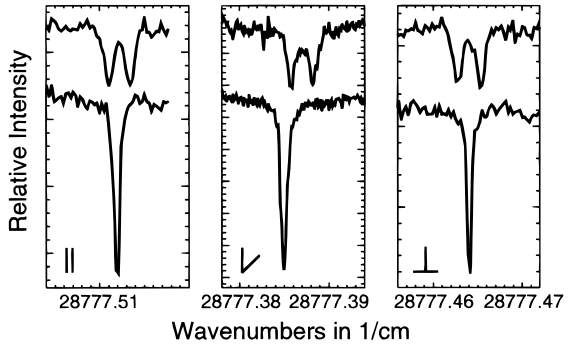

Figure 3. Example for anisotropic polarization dependence of hole profiles for octatetraene in *n*-heptane under an applied electric field (laser light polarized parallel to the applied field in the left panel, 45° in the center panel, and perpendicular to the applied field in the right panel). The lower scans show the original zero-field holes; the upper scans show the hole profiles under a 3.47 kV/cm applied field. The scans appear slightly shifted because of laser drift.

scopic models for geometry and charge distribution of these guest−host systems.

2. Experimental Section

2.1. Results. Holes burned into the lowest lying electronic singlet transition of randomly oriented, octatetraene-doped *n*-hexane microcrystals (full width approximately 5 cm^{-1} at 1.4 K) split when the laser light is polarized parallel to the applied electric field and broaden for a perpendicular polarization (Figure 2), reproducing the spectra recorded earlier.[7] Both effects are linear with respect to the electric field strength for experimentally attainable fields. Within the limits set by the experimental signal-to-noise ratio, the variation of the electric field effect is negligibly small over the inhomogeneous absorption band.[7]

In the case of octatetraene-doped *n*-heptane microcrystals (full width of the lowest lying singlet transition approximately 3 cm^{-1} at 1.4 K), the hole profile splits if the laser light is polarized parallel to the applied electric field. However, changing the laser polarization to a perpendicular configuration also reveals a hole splitting in some but not all cases (see Figure 3 for an example), a sign that the microcrystals are larger and render the irradiated sample volume anisotropic. Whether the hole splits or broadens if the laser light is polarized perpendicular to the applied field is different from case to case, although reproducible for the same hole. Anisotropy measurements support the idea of a preferred crystal orientation in the sample volume. Attempts to obtain

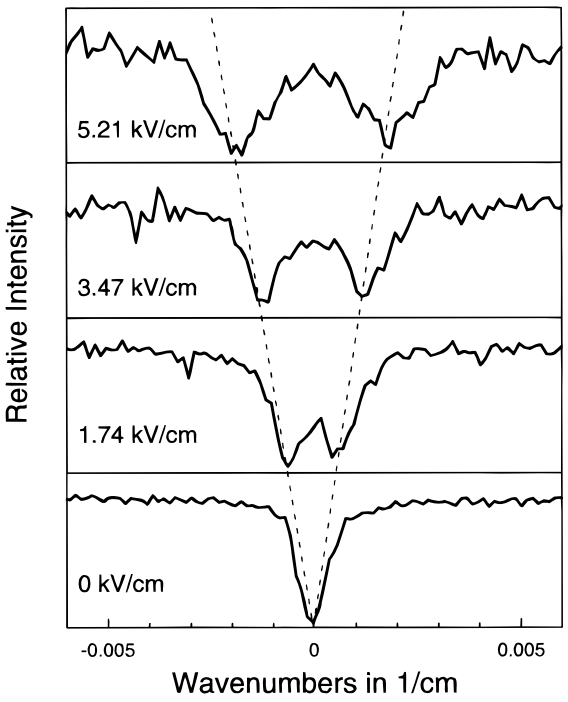

Figure 4. Dependence of the hole splitting in octatetraene-doped *n*-heptane on the applied electric field. The zero-field hole (bottom panel) was burned at 28 777.378 cm^{-1}, and the burning and scanning laser was polarized 45° relative to the external field. All scans were rescaled to the same peak intensity.

isotropic samples by grinding polycrystalline material under liquid nitrogen in an argon atmosphere have been unsuccessful because of small sample volume and complications from static electricity. All data, however, consistently give electric field effects that are about 3−4 times smaller than that in *n*-hexane. For the more than 20 holes burned into the inhomogeneously broadened absorption band, splitting and broadening effects for different laser polarizations are linear with respect to the attainable field strengths (up to 14 kV/cm). A typical case is shown in Figure 4. For the theoretical analysis of these field effects we choose only those data sets that show purely isotropic behavior.

2.2. Optical Setup and Sample Preparation. *Optical Setup.* Figure 5 shows the experimental setup, which follows those of earlier hole burning experiments in these systems. An argon ion laser (Coherent Sabre) pumps a tunable single frequency ring dye laser (Coherent 699-29) running on LD688 laser dye (Exciton). A LiO_3 intracavity doubling crystal produces close to 1 mW of tunable narrow bandwidth UV light in the region around 347−348 nm, which corresponds to the S_0-S_1 0−0 transition energy of octatetraene in *n*-hexane (28 744 cm^{-1}) and *n*-heptane (28 779 cm^{-1}).[8] To keep the active stabilization functional (measured rms frequency jitter of less than 500 kHz over several minutes), the normal 3% transmission output coupler is used instead of the 0.1% transmission output coupler recommended for UV operation. The light is passed through a half-wave plate that can rotate the laser polarization and irradiates the sample, which is contained in a 0.8 mm i.d., 0.3 mm thick melting point capillary (KIMAX-51, Kimball Products) in a glass cryostat with pumped liquid helium (Leybold Heraeus D60A backed WS250 pump, reducing the pressure to about 1 Torr, which corresponds to a temperature of 1.3 K). The external electric fields are generated by two parallel copper electrodes at a distance of about 1.4 mm that are connected to a high-voltage power supply (Bertan series 225).

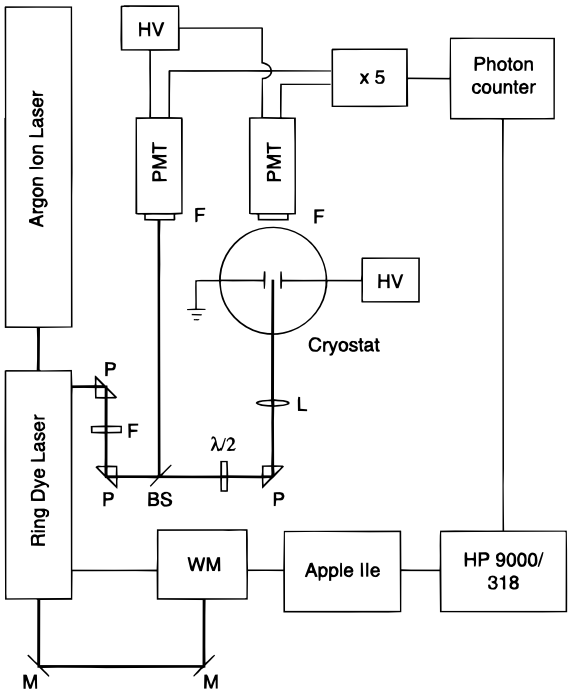

Figure 5. Experimental setup for hole burning in octatetraene-doped alkane crystals. Legend: M = mirror; P = quartz prism; F = filter; BS = beam splitter; $\lambda/2$ = half-wave plate; L = lens; PMT = photomultiplier tube; HV = high-voltage power supply; WM = wavemeter. Thick lines represent laser beams; thin lines show electrical connections.

For hole burning (typically 15 to 60 s), the laser is kept at a single frequency and the beam is slightly attenuated (intensity of about 0.3 mW/mm^2). For readout of the hole by fluorescence excitation, the laser is scanned at typically 10−100 times lower intensity to reduce additional burning effects. The fluorescence is detected by a cooled Burle C31000M photomultiplier tube through a cutoff filter chosen to transmit as much of the fluorescence spectrum as possible while blocking the scattered excitation light. Another cooled photomultiplier tube (EMI 625B) monitors the intensity of the exciting light for normalization purposes. The pulses from the two photomultiplier tubes are cleaned up using snubbers, preamplified, and collected by a two-channel photon counter (Stanford Research Systems SR400) that is interfaced to a Hewlett-Packard 9000/382 workstation as a data acquisition system. The latter also communicates with the Apple IIe (part of the Coherent Autoscan system), which was set up to transmit important scan data before each scan.

Sample Preparation. Octatetraene was taken from an *n*-pentane stock solution (stored at −10 °C) previously prepared according to the method given in ref 9. To remove impurities that had been accumulated over time and which showed UV absorption to the blue of octatetraene, a sample of 1 mL was processed through a 19 × 1.9 cm aluminum oxide (Woelm neutral, activity II, 3% H_2O) column using hexane Optima (Fisher) as an eluent.

To transfer octatetraene to the desired *n*-alkane solvent, 50 μL of the collected solution were injected into the HPLC system described in ref 7 operated with the desired *n*-alkane at a flow rate of 1 mL/min. The column was a LiChroCART Aluspher Al (5 μm particle size, 100 Å pore diameter; Merck) that was able to partially separate octatetraene isomers when 2.5% diethyl ether was added to the solvent.

The HPLC solvents were obtained as follows. *n*-Hexane was purified following a procedure adapted from ref 10. *n*-Hexane (Alfa; 99%) in an amount of 1 L was poured through a 2.4 cm diameter column filled to a length of 19 cm with $AgNO_3-Al_2O_3$ (about 150 g), which resulted in 800 mL pure solvent (the last 20% were discarded because of the column's limited capacity) in which the initial impurity with strong absorption from 200 to 290 nm was almost completely absent. HPLC grade *n*-heptane (99+%; Sigma-Aldrich) was used without further purification. Diethyl ether (B&J; contains preservative and ethanol) was purified by running it through a 20 cm long, 1 cm diameter column filled with neutral aluminum oxide (Woelm, activity II, 3% H_2O), which also removed the inhibitor (usually BHT, butylated hydroxytoluene, actual name 2,6-di-*tert*-butyl *p*-cresol, which causes absorption at <300 nm).

The absorbance at 302 nm (1 cm path length) of the final octatetraene samples was typically 2.2−6 for the *n*-hexane and *n*-heptane solutions. With a molar absorptivity of 5.3×10^4 L mol^{-1} cm^{-1},[9] this corresponds to concentrations of 40−100 μmol/L (1 octatetraene molecule per $\geq 10^5$ alkane molecules). The solutions were transferred into glass capillaries, sealed under argon, and lowered into liquid helium over the course of 15 min to obtain samples with high crystallinity.

3. Theory

3.1. Atomic Resolution Analysis. To analyze the experimental data, several approaches can be taken (for a review, see refs 11−13). Traditionally, a classical description for the energy of a polarizable, neutral particle with a permanent dipole moment in a homogeneous electric field is used to fit the experimental data.[14] Similarly, a quantum mechanical analysis at molecular resolution[7] can be invoked that is more accurate since it includes not only first- and second-order terms but higher order terms as well. Furthermore, the quantum mechanical approach yields information about the matrix environment (internal field), while the traditional interpretation of the classical equations only results in values for the induced dipole moment, a much more indirect measure of the properties of the molecular environment. Both methods, however, have one major drawback. They treat the molecule as a point object relative to the electric field (known as the point-dipole approximation in the quantum theory for the interaction of radiation with matter) and are thus not faithful to the real microscopic situation where the internal electrostatic fields vary dramatically over the volume of the probe molecule.

The quantum mechanical analysis at atomic resolution overcomes this obstacle and can be applied to any electrostatic potential distribution over the size of the molecule. Being completely general in its nature, it is applicable to a wide variety of quantum mechanical methods, not just Hückel theory as presented here, although this leads to especially simple modifications.

If we expose a system of n electrons (each having charge $-e$) and N nuclei (with individually differing charges $+eZ_A$) to an electrostatic field, the system's energy operator changes from $H^{(0)}$ to

$$H = H^{(0)} - e\sum_{i=1}^{n}\phi_i + e\sum_{A=1}^{N} Z_A\phi_A \qquad (1)$$

where ϕ_i and ϕ_A denote the electrostatic potentials due to this field at the location of electrons or nuclei, respectively. The Born−Oppenheimer approximation allows us to isolate the electronic problem

$$H_e = H_e^{(0)} - e\sum_{i=1}^{n}\phi_i \tag{2}$$

This operator forms the basis for the calculation of electronic energies under the influence of an electric field. Since it contains electron−electron repulsion terms, an exact mathematical solution is impossible, an obstacle known as electron correlation. In Hückel-type calculations, these electron−electron repulsion terms are replaced by some effective repulsive energy, leading finally to a separation of the electronic Hamiltonian into a set of (identical) one-electron Hamiltonians. Using the additional simplifying assumptions of Hückel theory, it can be rigorously shown[12] that in an electrostatic field the original Hückel Coulomb and resonance integrals, $\alpha_i^{(0)}$ and $\beta_{ij}^{(0)}$ (i and j being covalently linked atoms), have to be replaced by

$$\alpha_i = \alpha_i^{(0)} - e\langle\varphi_i|\phi|\varphi_i\rangle \tag{3}$$

and

$$\beta_{ij} = \beta_{ij}^{(0)} - e\langle\varphi_i|\phi|\varphi_j\rangle \tag{4}$$

The correction to the resonance integral, $\beta_{ij}^{(0)}$, can be neglected to first order since the overlap between bonded orbitals is relatively small (zero-differential overlap approximation).

What does this mean for the electronic energies of linear polyenes? Hückel calculations that consider bond length alternation by using empirical values for the resonance integrals of a single bond (β_s) and double bond (β_d) correctly predict the energy of the single-promotion state, which is actually the second excited singlet state (1^1B_u). The first excited singlet state (2^1A_g), however, is not well reproduced, which is attributed to the high degree of electron correlation.[15] This correlation error can be accounted for[15−17] by configuration interaction. The dominant part comes from the mixing of the doubly excited configuration (A_g2), created by the promotion of two electrons from the HOMO (highest occupied molecular orbital) to the LUMO (lowest unoccupied molecular orbital) and a linear combination of two double-jump promotions, A_g3 (promotion of one electron from HOMO to LUMO + 1 or from the HOMO − 1 to LUMO):

$$A_g2 = (\text{HOMO} \rightharpoonup \text{LUMO}, \overline{\text{HOMO} \rightharpoonup \text{LUMO}}) \tag{5}$$

$$A_g3 = 1/\sqrt{2}\,[(\text{HOMO} \rightharpoonup \text{LUMO} + 1) - (\text{HOMO} - 1 \rightharpoonup \text{LUMO})] \tag{6}$$

This type of configuration mixing is implemented in a Hückel model called HSS, Hückel Spectrum Simulator,[6] which accurately describes the electronic states of linear polyenes. It mixes the A_g2 and A_g3 configurations with an off-diagonal element of the form $(A+B)/N$, where N is the number of double bonds in the linear polyene and A and B are empirical values. The resonance integrals for single bonds and double bonds are expressed as $\beta_s = \beta_0 \exp(-\xi)$ and $\beta_d = \beta_0 \exp(+\xi)$, respectively. The four parameters β_0, ξ, A, and B, are fixed by fitting the experimentally available 0−0 excitation energies for different polyenes in low-temperature hydrocarbon solutions.

An extension of the HSS model for an atomic resolution analysis of electric field effects is now straightforward with the Coulomb integral correction given above. The expectation value for the potential ϕ at the location of the p orbital of atom i is approximated by its value at the nucleus, ϕ_i, which yields

$$\alpha_i = \alpha_i^{(0)} - e\phi_i \tag{7}$$

This model, named HSSISS (Hückel Spectrum Simulator including site shifts[18]) describes the excitation energies of linear polyenes in an arbitrarily complicated electric field if the electrostatic potentials at the carbon atoms of the π-electron system are known.

We should therefore be able to understand the electric field effect experiments if we know the set of potentials across the carbon backbone of octatetraene in the different alkane hosts. Even without external field, there exists an inhomogeneous, *internal* electric field or potential, $\mathbf{E}_{\text{int},P}$ and $\phi_{\text{int},P}$, respectively, at a given point P, which is generated by the molecular charge distributions of the surrounding matrix molecules. The average internal field or potential over the whole matrix is, of course, zero since the medium is not polarized and electrically neutral. This internal field or potential is modified, however, when an external electric field is applied. It polarizes the matrix, which leads to an *average* electric field inside the dielectric, $\mathbf{E}_{\text{diel}}$ (which can be different from the field given by voltage divided by the plate distance due to dielectric shielding of the sample holder and polarization charges on the sample surface). The consequences for field and potential at point P can be determined as follows (see Figure 6). We take a snapshot of the polarized material (i.e., freeze in the polarization) and carve out a macroscopic spherical cavity centered around this point, which is in a sense "virtual" since we do not allow the molecules to adjust their induced dipoles in response to the created vacuum. The field inside the empty cavity is higher than $\mathbf{E}_{\text{diel}}$ because of the polarization charges on the cavity surface. For the case of a uniformly polarized, isotropic dielectric (dielectric constant ϵ) and a cavity large enough to justify the use of continuum theory, the field inside the cavity is homogeneous and independent of the cavity radius. It is known as the Lorentz local field, $\mathbf{E}_{\text{Lor}} = ((\epsilon + 2)/3)\mathbf{E}_{\text{diel}}$. To this field we finally have to add the field or potential at point P created by the induced dipoles of the polarized material that we have just removed. We will refer to it as the (sphere) *polarization* field or potential, $\mathbf{E}_{\text{pol},P}$ and $\phi_{\text{pol},P}$, respectively. As for the case of the internal field or potential, it is inhomogeneous due to the anisotropy of the surrounding polarized material on this microscopic scale and its average together with the Lorentz field yields, of course, the average electric field inside the dielectric, $\mathbf{E}_{\text{diel}}$. Thus, the total electric field acting at a point P in the matrix is

$$\mathbf{E}_{\text{tot},P} = \mathbf{E}_{\text{int},P} + \mathbf{E}_{\text{pol},P} + \mathbf{E}_{\text{Lor}} \tag{8}$$

An equivalent expression holds for the corresponding potentials. However, since the Lorentz local field is constant everywhere in the sample, its corresponding potential changes linearly with the distance from the electrodes. We therefore write

$$\phi_{\text{tot},P} = \phi_{\text{int},P} + \phi_{\text{pol},P} - \int_O^P \mathbf{E}_{\text{Lor}}\,\mathrm{d}\mathbf{r} \tag{9}$$

where O is an arbitrary reference point for the Lorentz part to the potential.

3.2. Hole Profile Calculation. The basic formalism and details of this procedure have been described in a previous paper.[18] We now employ, more adequately, electrostatic potentials instead of field vectors to describe the effects of electric fields on electronic energies. The calculational procedure is briefly outlined below. First, the structure of the octatetraene site is determined by molecular mechanics calculations (see below). Second, the internal electrostatic potentials at the

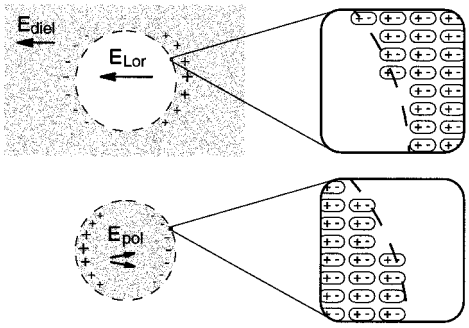

Figure 6. A dielectric sample is polarized by an externally applied electric field. Inside the dielectric, we find an average electric field $\mathbf{E}_{diel}$ that is, in general, different from the applied field (calculated as voltage divided by plate distance) due to polarization charges in the sample holder and on the dielectric surface (not shown). The microscopic field at a given point in the dielectric can be determined by first freezing in the polarization and then carving out a macroscopic, spherical cavity. It then has two components, the (homogeneous) Lorentz field inside the cavity (top) and the (inhomogeneous) field due to the polarized molecules inside the polarized sphere (below).

octatetraene carbon atoms, ϕ_{int}, are calculated by summing over the contributions of all *n*-alkane molecules whose centers are within 100 Å of the octatetraene impurity (typically about 25 000 alkane molecules). For this purpose, a *n*-alkane point charge model involving bonding electrons[18] is used that has only one adjustable parameter and is able to accurately reproduce the molecular electric potential at all distances outside the van der Waals radius. Third, to account for the matrix polarization effects of an externally applied electric field, the polarization potentials at the octatetraene carbon atoms, ϕ_{pol}, are calculated. Such calculations for three orthogonal directions of an applied field of fixed magnitude yield polarization potential tensors that determine the polarization potentials for arbitrary applied electric fields.

The hole profiles of polycrystalline samples are calculated as follows. For a given crystal orientation relative to the applied field, the polarization potentials for all octatetraene carbon atoms are determined from their polarization potential tensors. The Coulomb integrals are then adjusted according to the HSSISS model,

$$\alpha_i = \alpha_i^{(0)} - e(\phi_{int,i} + \phi_{pol,i}) + e\mathbf{E}_{Lor}\cdot(\mathbf{r}_i - \mathbf{r}_1) \qquad (10)$$

taking carbon atom 1 of octatetraene as the energy zero for the Lorentz field contribution. To account for the polycrystalline character of the samples, the lab coordinate system (containing the electric field vectors of the Lorentz field, $\mathbf{E}_{Lor}$, and of the laser polarization, $\boldsymbol{E}_{laser}$) is Euler rotated around the octatetraene molecule. Such a rotation is characterized by three angles relative to the molecular coordinate system: the polar and azimuthal angle of the applied field vector, ϑ and ζ, respectively, and the rotational angle, ω, of the laser light around this vector. For each orientation, the Coulomb integrals are evaluated and the transition energy shift (which is independent of the light vector and therefore needs to be calculated only once for all angles ω) relative to zero external field is computed using the HSSISS model. The intensity contribution, *I*, for a given orientation (ϑ,ζ,ω) is proportional to

$$I \propto (\mathbf{E}_{laser}\cdot\boldsymbol{\mu})^2(\mathbf{E}_{laser}\cdot\boldsymbol{\mu})^2 \sin\vartheta \qquad (11)$$

which contains the excitation probabilities for the burning and readout process ($\boldsymbol{\mu}$ is the S_0-S_1 transition dipole moment, approximated by the direction of the $1^1A_g - 1^1B_u$ transition calculated with the HSS model) and an orientational weighting factor. Each intensity-weighted transition energy shift is finally convolved with the Lorentzian line shape of the zero external field hole. The superposition of all orientational contributions gives the hole profile under the influence of an applied electric field.

3.3. Force Field. Since the geometry of the guest−host system forms the basis for the atomic resolution analysis, it is important to obtain sensible geometries for *n*-hexane and *n*-heptane crystals with octatetraene dopant molecules. Out of four force fields tested in the framework of the Cerius[2] molecular mechanics package (Cerius[2], version 1.6, Molecular Simulations Inc.), only the Universal Force Field, UFF,[19] was able to reproduce the bond alternation in all-*trans*-octatetraene crystals[20] and proved to describe the known crystal structures of *n*-hexane[21] and *n*-heptane[22] (with corrected values for C_2 $Z = 0.4594$, C_4 $Y = 0.2560$, and C_6 $Y = 0.3776$) most accurately.

Its parameters were optimized using the crystal structures of *n*-hexane, *n*-heptane, and all-*trans*-octatetraene as a training set, thereby preserving as much of the original force field parameter set as possible (see ref 23 for a list of changes to intramolecular parameters). By default, UFF uses a Lennard-Jones 6-12 type expression for van der Waals interactions. However, it has been shown in a recent comprehensive study of 20 van der Waals potentials for alkanes that two exp-6 type parameter sets yield the best results for various physical properties of alkanes in all three phases.[27] One of them, the MM3mc parameter set, was implemented in this work (using the suggested C−H bond shortening factor of 0.923 and applying the van der Waals terms for the alkane carbon atoms to the octatetraene carbon atoms types without any further changes).

Table 1 compares the average values for bond lengths and bond angles in *n*-hexane, *n*-heptane, and octatetraene from X-ray data to the values obtained from molecular mechanics simulations using the original and the modified UFF force field. It can be seen that, except for C−H bond lengths, which cannot be determined with high accuracy from X-ray data, all bond lengths are now predicted to within a few milliangstroms. Bond angles are, on average, accurate to within 0.1−0.2 deg (except for the unusually large hexane C−C−C angle), an improvement of an order of magnitude compared to the original UFF. A similar comparison of unit cell parameters, presented in Table 2, shows that the MM3mc van der Waals parameter set yields overall improved unit cell parameters.

3.4. Mixed Crystal Geometry. The aim of these simulations is to obtain a picture of the structure of octatetraene/alkane mixed crystals with one octatetraene on average surrounded by at least 10^5 alkane molecules. To mimic these conditions as closely as possible, the calculations are performed on infinite mixed crystal lattices consisting of superunit cells with one octatetraene replacing one or two alkane molecules in a $4 \times 4 \times 4$ alkane cluster (four alkane molecules in each of the unit cell directions; $5 \times 5 \times 5$ clusters are computationally much more expensive). That this cluster size is sufficient for this purpose is supported by the observation that, in the minimized structures, the alkane molecules further away from the octatetraene guest molecules remain in their positions that they occupy in the pure crystal.

To reduce the number of computational steps, the doped clusters are prepared from the minimized alkane structures rather than their crystallographic structures. Unit cell parameters are locked in these mixed crystal calculations in order to mimic the packing forces in a larger size alkane shell. The unit cell values are those of the minimized alkane structure (rather than

TABLE 1: Comparison of Average Values for Intramolecular Bond Lengths (in Å) and Bond Angles (in deg) in *n*-Hexane, *n*-Heptane, and Octatetraene Crystals[a]

			UFF		modified UFF	
type	system	X-ray value	value	Δ	value	Δ
C−C bonds	hex	1.527	1.529	0.002	1.528	0.001
	hep	1.528	1.529	0.001	1.528	0.000
	ot C=C	1.332	1.332	0.000	1.331	−0.001
	ot C−C	1.451	1.470	0.019	1.450	−0.001
C−H bonds	hep	1.000	1.112	0.112	1.048	0.048
	ot terminal hor	0.970	1.082	0.112	1.017	0.047
	ot terminal perp	1.029	1.085	0.056	1.019	−0.010
C−C−C angles	hex	113.8	110.5	−3.3	113.1	−0.7
	hep	113.2	110.5	−2.7	113.2	0.0
	ot	125.0	120.9	−4.1	125.1	0.1
H−C−C angles	hep methyl	109.2	110.6	1.4	109.3	0.1
	hep methylene	108.7	109.6	0.9	108.7	0.0
	ot H−C−C	115.4	119.4	4.0	115.6	0.2
	ot H−C=C	119.8	120.1	0.3	119.9	0.1
H−C−H angles	hep methyl	109.7	108.4	−1.3	109.7	0.0
	hep methylene	108.9	108.0	−0.9	109.0	0.1
	ot	118.3	118.5	0.2	118.5	0.2

[a] Hex = *n*-hexane, hep = *n*-heptane, ot = octatetraene, terminal hor = terminal C−H bonds pointing along the chain axis, terminal perp = terminal C−H bonds perpendicular to the chain axis.

TABLE 2: Comparison of Unit Cell Dimensions in *n*-Hexane, *n*-Heptane, and Octatetraene Crystals (*a*, *b*, and *c* in Å, α, *β*, and *γ* in deg)]

	unit	X-ray	UFF		modified UFF	
system	cell	value	value	Δ	value	Δ
n-hexane	*a*	4.17	4.18	0.01	4.15	−0.02
	b	4.70	4.46	−0.24	4.47	−0.23
	c	8.57	8.53	−0.04	8.53	−0.04
	α	96.6	97.2	0.6	95.4	−1.2
	β	87.2	89.4	2.2	87.8	0.6
	γ	105.0	102.2	−2.8	105.2	0.2
n-heptane	*a*	4.15	4.17	0.02	4.14	−0.01
	b	19.97	19.75	−0.22	19.93	−0.04
	c	4.69	4.46	−0.23	4.46	−0.23
	α	91.3	91.1	−0.2	91.4	0.1
	β	74.3	77.9	3.6	74.2	−0.1
	γ	85.1	86.6	1.5	86.4	1.3
octatetraene	*a*	10.23	9.92	−0.31	10.18	−0.05
	b	4.12	3.92	−0.20	4.08	−0.04
	c	8.31	8.53	0.22	8.28	−0.03
	α	90.0	90.1	0.1	89.7	−0.3
	β	96.5	96.0	−0.5	96.1	−0.4
	γ	90.0	90.0	0.0	89.9	−0.1

the crystallographic unit cell) to avoid artifacts due to the creation of empty space or artificial stresses that would primarily affect the octatetraene geometry in the host cavity. The charge equilibration method[24] cannot be used with these lattices because of the size of the calculations. Therefore, atomic point charges are fixed to their values in the pure crystals (obtained there using the charge equilibration method).

The first attempts of mixed crystal minimizations have shown that the octatetraene molecule does not have a chance to relax in the host cavity before the default termination criterion of 0.1 kcal/mol/Å rms force (the *average* net force per atom) is met. With more than 60 alkane molecules per unit cell occupying positions that are already fairly relaxed, not enough emphasis is placed on the single octatetraene molecule with a relatively strained initial position. On the other hand, calculations with a termination criterion of only 0.001 kcal/mol/Å rms force fail to converge within 1000 steps. To solve this problem, a two-fold approach is taken. The convergence criterion is reduced only 10-fold (0.01 kcal/mol/Å), and most importantly, the locations of all alkane atoms are fixed during the first computational stage. Now the octatetraene molecule alone has to meet the rms force criterion by adjusting its position and

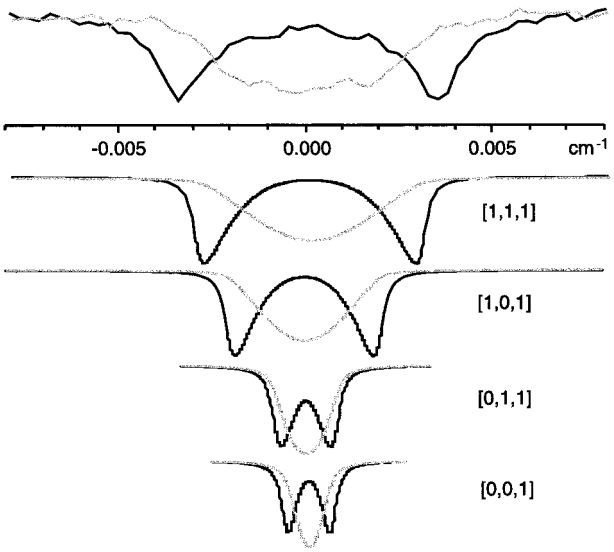

Figure 7. Experimental (top) and calculated hole profiles for octatetraene in *n*-hexane under an applied electric field of 2.78 kV/cm (voltage divided by plate distance). Gray lines represent a perpendicular laser polarization with respect to the applied field; black lines are for parallel polarization. An almost quantitative agreement is obtained for the [1,1,1] site, without even changing the only adjustable parameter of this model, namely the overall scaling factor for the *n*-alkane charge model. All profiles were rescaled to yield the same peak intensities.

geometry under the influence of the frozen alkane matrix. This first minimization stage is from now on referred to as the *octatetraene relaxation stage* (or *guest relaxation stage* in general). The Spline method (falling off over the region 18−20 Å) is used for nonbond interactions to reduce the computation time.

The results from these calculations are then fed to the second stage calculations where the alkane molecules are allowed to fully relax. This complete minimization is carried out under the same conditions that optimized the pure crystal structures of octatetraene, *n*-hexane, and *n*-heptane (Ewald summation[25,26] for long-range nonbond interactions and the default termination criterion of 0.1 kcal/mol/Å rms force) to ensure sensible results. However, the unit cell is kept fixed for reasons described above, and fixed values for atomic point charges must be used because of the system's size. Since the main effect of this second

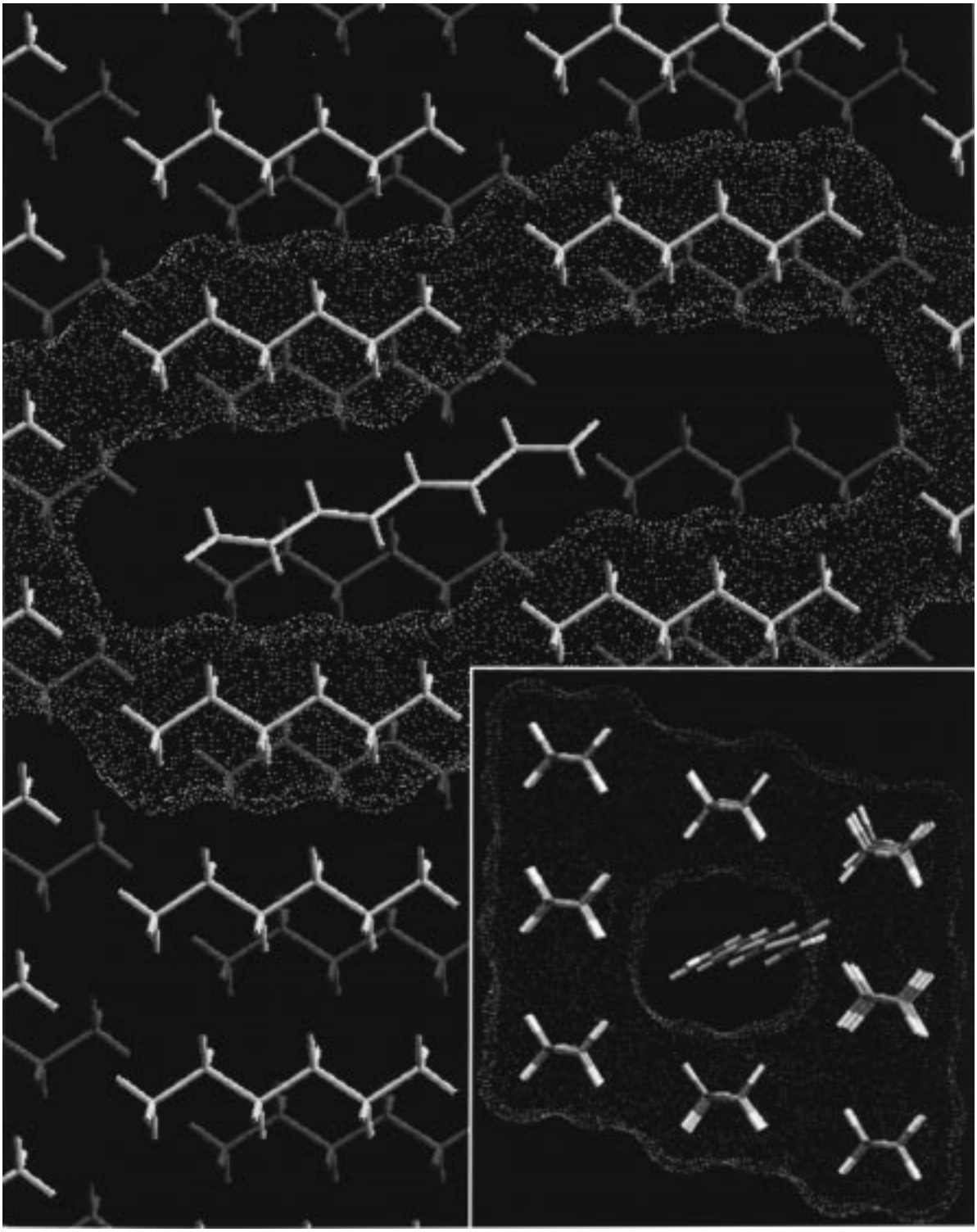

Figure 8. Geometry of the minimized [1,1,1] hexane site accommodating the octatetraene molecule. The cavity is outlined by the 1.4 Å Connolly surface of the adjacent hexane molecules, which shift only very slightly from their normal positions. The internal electric potentials at the octatetraene carbon atoms are (from left to right) −8.24, −3.78, −7.26, −4.26, 28.69, 13.70, 6.36, and 13.10 mV, which demonstrates how inhomogeneous the corresponding internal electric fields are. A side view of the cavity is presented in the inset on the lower right, showing that the octatetraene molecule is slightly twisted around its long axis in response to the crystal packing forces.

minimization stage is to relax the alkane matrix around the octatetraene cavity, it is referred to as the *matrix relaxation stage*. It is the final step in the mixed crystal minimizations, yielding the exact positions of the octatetraene carbon atoms relative to the alkane host matrix.

3.5. Fields and Potentials. The details of the calculation of internal fields and potentials is given elsewhere.[18] Only two important points should be mentioned here. By assuming that all alkane molecules are represented by the same point charge distribution regardless of their distance to the octatetraene molecule, we are implicitly neglecting any reaction field effects (polarization of surrounding alkane molecules due to the dipole moment of the octatetraene impurity in the matrix). Also, because we use vacuum electrostatics to calculate the fields and potentials (no screening of fields due to dielectric material between the field source and the point of interest), our charge

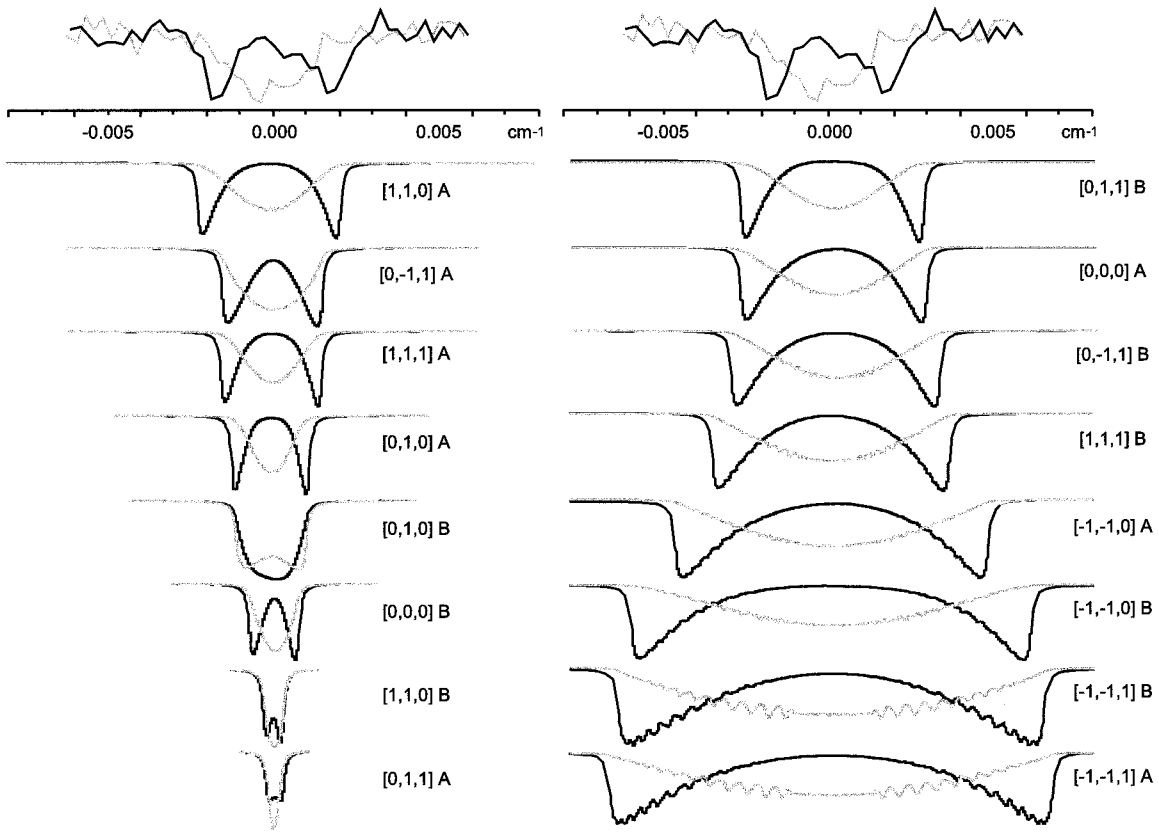

Figure 9. Experimental (top) and calculated hole profiles for octatetraene in *n*-heptane under an applied electric field 2.5 times higher than that of the *n*-hexane case, namely 6.94 kV/cm (voltage divided by plate distance). Gray lines represent a perpendicular laser polarization with respect to the applied field; black lines are for parallel polarization. The [1,1,0] A site shows the best agreement with the experiment. The overall scaling factor for the *n*-alkane charge model used in the calculation is 1.0. All profiles were rescaled to yield the same peak intensities.

model represents the charge distribution of an *n*-alkane *in its crystal environment*, in contrast to the point charge model for isolated *n*-alkane molecules developed in ref 28.

For the calculation of polarization potentials, we first have to take into account the dielectric shielding of the glass capillary that contains the sample. Using a low-temperature dielectric constant of $\epsilon_1 = 2.33$ for *n*-hexane[7] and *n*-heptane, $\epsilon_2 = 4.05$ for borosilicate glass (estimated from high-frequency data at −50 °C and 10^{10} Hz[32]), and a capillary with an inner radius of 0.44 mm and an outer radius of 0.70 mm, we obtain a homogeneous field $\mathbf{E}_{\text{diel}}$ inside the sample of (see ref 12 or footnote 18 in ref 29)

$$\mathbf{E}_{\text{diel}} = 0.54\mathbf{E}_{\text{ext}} \tag{12}$$

which yields for the Lorentz cavity field

$$\mathbf{E}_{\text{Lor}} = ((\epsilon_1 + 2)/3)\mathbf{E}_{\text{diel}} = 0.78\mathbf{E}_{\text{ext}} \tag{13}$$

By using a scalar instead of a tensor for the dielectric constant, we make the assumption that the matrix outside the cavity is isotropic. This is only partly true even if we assume that the macroscopic cavity is of the size of a microcrystal that is surrounded by a randomized ensemble of other microcrystals. However, the error made in this assumption is small. The homogeneous field in the Lorentz cavity polarizes the molecules inside this sphere, and we use our microscopic model for the octatetraene environment to calculate these polarization effects using bond polarizabilities from refs 30 and 31 and the *n*-alkane point charge model mentioned above. Details of the calculation can be found in ref 18, which however, neglects the shielding factor of 0.78.

4. Results

4.1. Octatetraene in *n*-Hexane. Since an octatetraene molecule is significantly longer than *n*-hexane, it only fits in a vacancy in the host crystal that is created by removing two vicinal alkane molecules. This leaves us with a number of possible guest−host geometries that need to be investigated separately, only one of which reflects the real situation. To reduce the number of possibilities, it is reasonable to assume that octatetraene is aligned along the hexane chains. A detailed analysis of all possible cavities shows that only four two-molecule cavities are able to accommodate an octatetraene molecule. They are labeled [0,0,1], [0,1,1], [1,0,1], and [1,1,1], indicating the position of the second alkane molecule (in terms of the unit cell vectors *a*, *b*, and *c*) that is replaced by the octatetraene molecule. The first alkane molecule is always the center molecule, [0,0,0].

In each of these four different cavities, octatetraene can have zigzag or zagzig orientation relative to the alkane chain and can occupy different translationally related positions in the cavity. Since a total minimization traps the octatetraene molecule in a local minimum before it can sample these positions, different input structures need to be considered. Shifting the octatetraene molecule in 1 Å steps along the main cavity direction results in 10 different octatetraene configurations for each of the four two-molecule cavities or a total of 40 different input structures sampling the configurational space. The octatetraene relaxation stage of the molecular mechanics minimization reduces the number of distinguishable sites from 40 to 26. The convergence of structures is an indication that the octatetraene relaxation stage is properly set up to give the intended results and that a sampling of the translational subspace

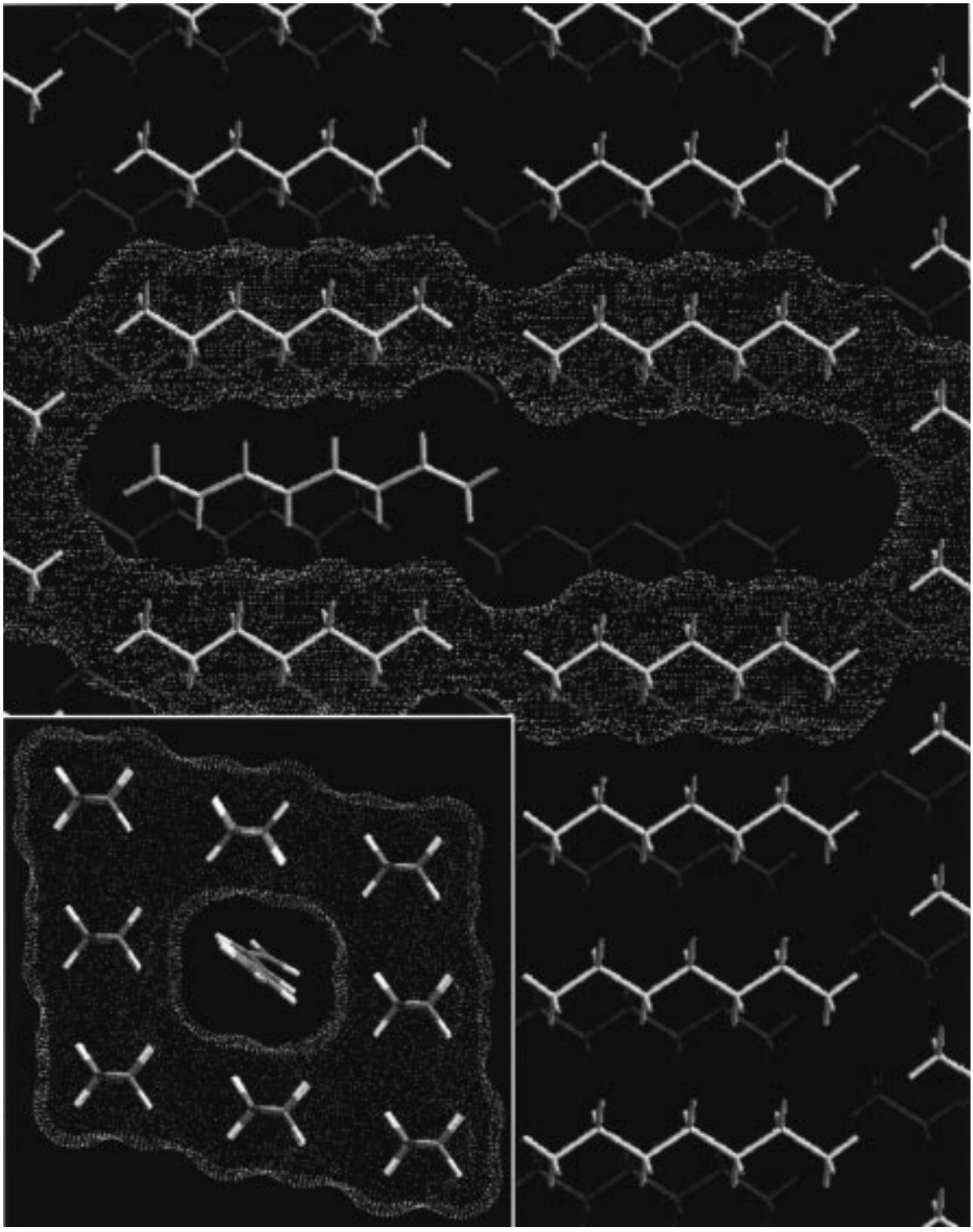

Figure 10. Geometry of the minimized [1,1,0] A heptane site accommodating the octatetraene molecule, together with the 1.4 Å Connolly surface outlining the cavity. The internal electric potentials vary again over the size of the octatetraene carbon backbone but to a lesser degree than in the hexane site presented earlier (from left to right: −25.8, −28.5, −21.2, −25.3, −26.7, −21.6, −37.7, and −28.8 mV). A side view of the cavity is presented in the inset on the lower left, showing that the octatetraene molecule is bent in the cavity in order to avoid bad van der Waals contacts.

in 1 Å steps is appropriate. The two lowest energy configurations of each of the four cavities are subjected to the matrix relaxation stage. Any resulting structures with inversion symmetry are discarded since the one-photon hole burning experiments are blind to centrosymmetric structures even if they exist. This leaves only one structure for each of the four cavities to be considered for the hole profile calculations.

For all four possible candidates, the hole profiles calculated with the HSSISS model described above are presented in Figure 7. It is amazing how differently the four sites respond to an applied electric field, demonstrating just how sensitive Stark experiments are to the probe molecule's nanoenvironment and that, in return, only a microscopic analysis can lead to an understanding of the observed effects. The [1,1,1] site, where octatetraene replaces two *n*-hexane neighbors along the unit cell diagonal, shows the best agreement with the experimental data. Figure 8 presents the structure of the host cavity with the octatetraene guest molecule. It can be seen that the latter is

TABLE 3: Possible Combinations of Octatetraene Sites in *n*-Hexane (hex) and *n*-Heptane (hep)[a]

hex	[1,1,1]	[1,1,1]	[1,1,1]	[1,1,1]	[1,0,1]	[1,0,1]	[1,0,1]	[1,0,1]
hep	[1,1,0] A	[1,1,1] A	[0,−1,1] A	[0,1,0] A	[1,1,1] A	[0,−1,1] A	[0,1,0] A	[0,0,0] B
f	1.00	1.25	1.30	1.40	1.50	1.60	1.70	2.20

[a] The listed pairs would, along with the proper scaling factor *f* for the alkane charges, lead to an agreement in energy shifts of better than 20% compared with the experimental hole profiles. It was hereby assumed that the uncertainty in the originally chosen point charges for the alkane charge model does not exceed a factor of 4.

slightly twisted along its main axis due to crystal packing forces. All of the resulting guest−host geometries show that the alkane molecules adjacent to the octatetraene shift only slightly from their normal positions. In other words, the cavity does not collapse around the octatetraene molecule; the intermolecular attractions to the neighboring alkane molecules of the crystal lattice hold the cavity lining molecules in place. Alkane molecules further away from the octatetraene molecule remain in the positions that they occupy in the pure hexane crystal.

4.2. Octatetraene in *n*-Heptane. Octatetraene is only slightly longer than *n*-heptane, so both single-molecule and two-molecule vacancies have to be considered. The situation is further complicated by the fact that *n*-heptane has a unit cell with two molecules, which have different environments and are therefore not equivalent. This results in one single-molecule cavity and eight two-molecule cavities that need to be considered for further analysis. They are labeled by the position of the second alkane molecule (in terms of the vectors *a*, *b*/2, and *c*) that is replaced by the octatetraene molecule. On the analogy of the *n*-hexane case, two octatetraene orientations need to be looked at for the single-molecule cavity (zigzag and zagzig). This is also true for the two-molecule cavities, where in addition six different 1 Å step translational configurations have to be taken into account, which makes 12 configurations for each of the eight two-molecule cavities. This yields a total of 98 input structures sampling the configurational space of this system.

The octatetraene relaxation stage reduces this number from 98 to 56, and the matrix relaxation stage of the molecular mechanics simulation is carried out on the two lowest energy configurations for each cavity. They are labeled A and B, where A is the structure with the lower energy. The results of the calculated hole profiles for all minimized structures are presented in Figure 9. For comparison, an experimental hole profile for an isotropic sample has been chosen. The best match is a structure where the octatetraene guest replaces two *n*-heptane molecules along the (a,b/2) diagonal (Figure 10). In contrast to the hexane structure, the splitting here is slightly larger than that in the experiment. However, the differences between measured and calculated profiles are in both cases not very significant so that, to within the simulation error, the agreement can be called quantitative.

It should also not be forgotten that the model contains one adjustable parameter, namely the overall scaling parameter of the *n*-alkane charge model. By choosing this value appropriately, other sites in both hosts can give a quantitative agreement with the experiments. These possibilities are listed in Table 3 along with the corresponding value of the scaling factor. The final goal of identifying the exact guest−host structure and determining the charge distribution in *n*-alkanes requires therefore still more experimental information to consider. This work is currently in progress. However, it should not be underestimated what has already been achieved, namely explaining, on a fundamental level, the strikingly different Stark behavior of the octatetraene probe molecule in two *n*-alkane hosts with identical bulk dielectric properties.

5. Conclusion

This paper presents a general model for the effect that an arbitrary electrostatic field distribution over the size of a probe molecule has on molecular electronic energy levels. Applied to Hückel-type models, this leads to especially simple modifications. Such a model, the HSSISS model for linear polyene electronic structure in an electrostatic field, is used in a scheme for analyzing experiments that study the effects of an external electric field on persistent holes burned into the lowest lying electronic singlet transition of octatetraene in two alkane hosts, *n*-hexane and *n*-heptane. Structure is obtained from molecular mechanics calculations with a modified Universal force field that accurately reproduces the crystal structures of *n*-hexane, *n*-heptane, and all-*trans*-octatetraene. Internal and polarization fields and potentials are calculated by classical electrostatics based on a point charge model for *n*-alkanes and bond polarizabilities from literature, and hole profiles are calculated for comparison with the experimental results. There is only one adjustable parameter in this procedure, namely the overall scaling parameter of the *n*-alkane charge model. For both alkane hosts, an excellent agreement with the experiment can be obtained for selected structures. There are several reasons that make us confident that the proposed structures and the analysis scheme are correctly reflecting the real microscopic situation. The procedure is based on an accurate model for linear polyene electronic structure that properly predicts the changes upon addition of double bond units, which is certainly a more dramatic perturbation than the application of an electrostatic field to the molecule. Second, the structure determination is based on a force field that correctly reproduces the structures of the pure molecular crystals so that sensible results can also be expected for the mixed crystal calculations. Furthermore, the analysis of the effects that electrostatic fields and potentials have on electronic energies contains no crude simplifications. Thus, all aspects of the treatment are consistent with the detailed, microscopic structure of the guest−host system.

Acknowledgment. This work was supported by grants from the NSF (CHE-9417103) and the NIH (EY06466).

References and Notes

(1) *Persistent Spectral Hole-Burning: Science and Applications*; Moerner, W. E., Ed.; Springer: Berlin, 1988.

(2) Kohler, B. E. *Chem. Rev.* **1993**, *93*, 41.

(3) Granville, M. F.; Holtom, G. R.; Kohler, B. E. *Proc. Natl. Acad. Sci. U.S.A.* **1980**, *77*, 31.

(4) Ackerman, J. R.; Huppert, D.; Kohler, B. E.; Rentzepis, P. M. *J. Chem. Phys.* **1982**, *77*, 3967.

(5) Kohler, B. E.; Snow, J. B. *J. Chem. Phys.* **1983**, *79*, 2134.

(6) Kohler, B. E. *J. Chem. Phys.* **1990**, *93*, 5838.

(7) Gradl, G.; Kohler, B. E.; Westerfield, C. *J. Chem. Phys.* **1992**, *97*, 6064.

(8) Snow, J. Ph.D. Thesis, Wesleyan University, 1980.

(9) Spangler, C.; Little, D. A. *J. Chem. Soc., Perkin Trans.* **1982**, *1*, 2379.

(10) Murray, E.; Keller, R. *J. Org. Chem.* **1969**, *34*, 2234.

(11) Kohler, B. E.; Personov, R. I.; Woehl, J. C. In *Laser Techniques in Chemistry*; Myers, A. B., Rizzo, T. R., Eds.; John Wiley: New York, 1995; Chapter 8.

(12) Woehl, J. C. Ph.D. Thesis, University of California Riverside, 1996 (available through UMI Dissertation Services).
(13) Kohler, B. E.; Woehl, J. C. *Mol. Cryst. Liq. Cryst.* **1996**, *291*, 119.
(14) Samoilenko, V. D.; Razumova, N. V.; Personov, R. I. *Opt. Spectrosc.* **1982**, *52*, 346.
(15) Schulten, K.; Karplus, M. *Chem. Phys. Lett.* **1972**, *14*, 305.
(16) Hudson, B. S.; Kohler, B. E.; Schulten, K. *Excited States* **1982**, *6*, 1.
(17) Ohmine, I.; Karplus, M.; Schulten, K. *J. Chem. Phys.* **1978**, *68*, 2298.
(18) Kohler, B. E.; Woehl, J. C. *J. Chem. Phys.* **1995**, *102*, 7773; (addendum) *J. Chem. Phys.* **1996**, *104*, 3148.
(19) Rappé, A. K.; Casewit, C. J.; Colwell, K. S.; Goddard, W. A., III; Skiff, W. M. *J. Am. Chem. Soc.* **1992**, *114*, 10024.
(20) Baughman, R. H.; Kohler, B. E.; Levy, I. J.; Spangler, C. *Synth. Met.* **1985**, *11*, 37.
(21) Norman, N.; Mathisen, H. *Acta Chem. Scand.* **1961**, *15*, 1755.
(22) Merle, A. *Chem. Phys.* **1977**, *22*, 207.
(23) The systematic approach was to change the stiffest terms first since they have a more dramatic influence on softer terms than vice versa. The UFF is built on the idea that a small set of generator parameters defines the large set of parameters for the energy terms. Therefore, major adjustments to generator parameters were avoided, and specific energy terms were rather defined explicitly (overriding the energy term created by the generator set). This was done in a way such that the established general rules were obeyed that connect parameters of the same energy term among each other and to the generator set, making any changes consistent with the UFF approach. The modifications were as follows. (a) New atom types for the sp^2 hybridized carbon atoms of octatetraene, C_R1 and C_R2, were created, representing octatetraene as C_R1═C_R2−C_R2═C_R1−C_R1═C_R2−C_R2═C_R1, with generator parameters identical to those of C_R. (b) The C_R1 and C_R2 valence bond radii were changed from 0.729 to 0.7305 Å. (c) The bond order for C−C single bonds in octatetraene (C_R1−C_R1 and C_R2−C_R2) was set to $n = 1.09$. (d) The C_3 valence bond radius was changed from 0.757 to 0.759 Å. (e) The H_ valence bond radius was changed from 0.354 to 0.286 Å. (f) The C−C═C equilibrium bond angle in octatetraene (C_R1−C_R1═C_R2 and C_R1═C_R2−C_R2) was changed from 120.0° to 125.0° (three-term Fourier expansion with $\theta_0 =$ 125.0° and $K = 198.1177$ kcal/mol). (g) The C−C−C equilibrium bond angle in alkanes was changed from 109.47° to 113.5° (three-term Fourier expansion with $\theta_0 = 113.5°$ and $K = 192.9321$ kcal/mol). (h) The H−C═C equilibrium bond angle in octatetraene (H_−C_R1═C_R2 and H_−C_R2═C_R1) was changed from 120.0° to 119.6° (three-term Fourier expansion with $\theta_0 = 119.6°$ and $K = 132.5348$ kcal/mol). (i) The H−C−C equilibrium bond angle in octatetraene (H_−C_R1−C_R1 and H_−C_R2−C_R2) was changed from 120.0° to 115.9° (three-term Fourier expansion with $\theta_0 = 115.9°$ and $K = 121.3549$ kcal/mol). (j) The H−C−C equilibrium bond angle in alkanes was changed from 109.47° to 108.15° (three-term Fourier expansion with $\theta_0 = 108.15°$ and $K = 126.5625$ kcal/mol). (k) The H−C−H equilibrium bond angle in octatetraene (H_−C_R1−H_) was changed from 120.0° to 118.4° (three-term Fourier expansion with $\theta_0 =$ 118.4° and $K = 78.4565$ kcal/mol). (l) The H−C−H equilibrium bond angle in alkanes was changed from 109.47° to 110.5° (three-term Fourier expansion with $\theta_0 = 110.5°$ and $K = 86.6293$ kcal/mol).
(24) Rappé, A. K.; Goddard, W. A., III *J. Phys. Chem.* **1991**, *95*, 3358.
(25) Ewald, P. *Ann. Phys.* **1921**, *64*, 253.
(26) Karasawa, N.; Goddard, W. A., III *J. Phys. Chem.* **1989**, *93*, 7320.
(27) Nagy, J.; Weaver, D. F.; Smith, V. H., Jr. *J. Phys. Chem.* **1995**, *99*, 8058.
(28) Chipot, C.; Ángyàn, J. G.; Ferenczy, G. G.; Scheraga, H. A. *J. Phys. Chem.* **1993**, *97*, 6628.
(29) Geissinger, P.; Kohler, B. E.; Woehl, J. C. *J. Phys. Chem.* **1995**, *99*, 16527.
(30) Landolt-Börnstein. *Atom- und Molekularphysik*, 6th ed.; Springer: Berlin, 1951; Vol. I/3.
(31) Denbigh, K. G. *Trans. Faraday Soc.* **1940**, *36*, 936.
(32) *Dielectric Materials and Applications*; Hippel, A. V., Ed.; John Wiley: New York, 1954.